Author(s): Puttreddy, Rakesh; Rautiainen, J. Mikko; Yu, Shilin; Rissanen, Kari

Title: N−X···O−N Halogen Bonds in Complexes of N-Haloimides and Pyridine-N-oxides : A Large Data Set Study

Year: 2023

Version: Published version

Please cite the original version:

Puttreddy, R., Rautiainen, J. M., Yu, S., & Rissanen, K. (2023). N−X···O−N Halogen Bonds in Complexes of N-Haloimides and Pyridine-N-oxides : A Large Data Set Study. Angewandte Chemie, 62(34), Article e202307372. https://doi.org/10.1002/anie.202307372

How to cite: *Angew. Chem. Int. Ed.* **2023**, *62*, e202307372
doi.org/10.1002/anie.202307372

Halogen Bonding

N–X···O–N Halogen Bonds in Complexes of *N*-Haloimides and Pyridine-*N*-oxides: A Large Data Set Study

Rakesh Puttreddy, J. Mikko Rautiainen, Shilin Yu, and Kari Rissanen**

Abstract: N–X···$^{-}$O–N^{+} halogen-bonded systems formed by 27 pyridine N-oxides (PyNOs) as halogen-bond (XB) acceptors and two N-halosuccinimides, two N-halophthalimides, and two N-halosaccharins as XB donors are studied in silico, in solution, and in the solid state. This large set of data (132 DFT optimized structures, 75 crystal structures, and 168 ^{1}H NMR titrations) provides a unique view to structural and bonding properties. In the computational part, a simple electrostatic model (SiElMo) for predicting XB energies using only the properties of halogen donors and oxygen acceptors is developed. The SiElMo energies are in perfect accord with energies calculated from XB complexes optimized with two high-level DFT approaches. Data from in silico bond energies and single-crystal X-ray structures correlate; however, data from solution do not. The polydentate bonding characteristic of the PyNOs' oxygen atom in solution, as revealed by solid-state structures, is attributed to the lack of correlation between DFT/solid-state and solution data. XB strength is only slightly affected by the PyNO oxygen properties [(atomic charge (Q), ionization energy ($I_{s,min}$) and local negative minima ($V_{s,min}$)], as the σ-hole ($V_{s,max}$) of the donor halogen is the key determinant leading to the sequence N-halosaccharin > N-halosuccinimide > N-halophthalimide on the XB strength.

Introduction

Non-covalent interactions (NCIs) play a crucial role in preserving the structural integrity of numerous chemical[1] and biological[2,3] systems. For example, nature creates a diverse range of proteins using the same set of 20 amino acids that differ only in their side chains. These side chains induce and support a wide range of NCIs including hydrogen bonds (HBs) and ionic bonds, manifesting large structural and functional diversity.[4] Due to the paramount significance of NCIs, extensive research has been conducted to elucidate and quantify various NCI motifs, which are broadly classified into four categories;[5] van der Waals forces, dipole-dipole interactions, electrostatic interactions, and ionic bonds (Figure 1). The strengths of these NCIs vary greatly, spanning over a wide range. At the one end of the spectrum, there are weak NCIs such as the hydrophobic effect (< 5 kJ mol^{-1}), while the opposite end of the spectrum are the electrostatic interactions, namely, ionic bonds (> 500 kJ mol^{-1}). Those in the middle of the interaction spectrum, such as hydrogen and halogen bonds (XB) (~0.5- > 200 kJ mol^{-1}), have received broad interest because they are ubiquitous in nature and are, together with metal coordination, the key tools in the creation of complex supramolecular systems.[6]

Both HBs and XBs are reversible, and often multiple HBs and XBs are required to provide structural integrity and stability to supramolecular materials.[6] The seminal work of Margaret Etter et al.[7] has shown that strong HBs are a reliable design tool for assembling molecules into high fidelity supermolecules and supramolecular structures. Since these early studies, a supramolecular approach has been extensively used to investigate the breadth, scope, and the importance of HBs in co-crystals or molecular supramolecular complexes. According to Jeffrey[8] HBs can be broadly categorised into weak, moderate and strong based on the nature of the donor-acceptor pairs[9] and interaction energies; (1) weak HBs of < 16 kJ mol^{-1}, generally formed between soft acids and soft bases (e.g., C–H···π, C–H···S), have nearly the same strength as dipole-dipole interactions. (2) Moderate HBs (16–67 kJ mol^{-1}), which are most common and abundant, are formed by combining one hard acid and one soft base component or vice versa (e.g., N–H···O, N–H···halogen). (3) Strong HBs (67- >

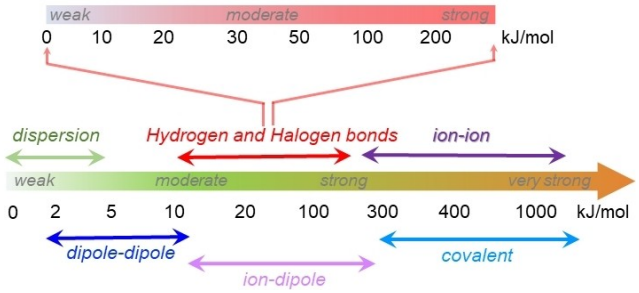

Figure 1. General hierarchy of chemical bonding.

[*] R. Puttreddy, J. M. Rautiainen, S. Yu, K. Rissanen
University of Jyvaskyla, Department of Chemistry
P.O. BOX 35, 40014 Jyväskylä (Finland)
E-mail: rakesh.r.puttreddy@jyu.fi
kari.t.rissanen@jyu.fi

167 kJ mol^{-1}) formed between hard acids and hard bases (e.g., [F···H···F]$^+$, [N···H···N]$^+$) are as strong as half the strengths of covalent bonds. The HB and most recently also XB toolbox has now matured to a point where structures of any strength can be modelled and attributed to rationalize chemical transformations ranging from simple organic reactions[10] to polymers[11] as well as to explain the functional properties of materials.[12]

Halogen bonding[13] is the newest member of the mid-spectrum interactions family and a very close relative of HB.[14,15] Although XB and HB are comparable in many aspects, the differences between the two has boosted the XB research. There are at least three obvious differences between XB and HB. First, the polarization and thus XB strength of the halogen follows the order I > Br > Cl ⩾ F, on a given system D–X···A (D = any atom that can polarize the X; X = electron-deficient I, Br or Cl; A = electron-rich atom, an XB acceptor).[16] Second, modulating the electron-withdrawing nature of D the electron-deficient area (so called σ-hole[17,18]) can be tuned.[19] Finally, the halogen participating in the XB creates a highly directional halogen bond due to the electron-deficient area (σ-hole) on the extension of the D–X bond.[17] The σ-hole imposes constraints to bonding and linearity of the geometries of XB interactions, allowing design and construction of specific molecular structures and materials for targeted applications.[20,21] The X···A halogen bonding motif manifests a wide range of interaction energies, from weak (~0.5–20 kJ mol^{-1}) to moderate (~20–60 kJ mol^{-1}) and strong (~ > 60 kJ mol^{-1}) to be utilized in a multitude of applications.[20,21] The development of the halogen σ-hole theory and its directionality have significantly broadened our understanding of non-covalent interactions, moving beyond the recently discovered chalcogen bonding[22] to a whole new palette of previously unforeseen interactions like aerogen,[23] spodium,[24] pnictogen,[25] tetrel,[25] and triel[26] bonds. Although applications are less obvious, these late-discovery interactions have enormous technical potential in areas like catalysis, anion recognition, and medicinal chemistry.[25,27–30]

The weak and moderate XBs of C–I···N type, formed by iodoperfluoroalkane/arenes and N-heterocycles, have been used in functional materials[31] owing to their reversible nature, whereas the strong [N–I–N]$^+$ 3-*center*-4-*electron* halogen bonds stabilize the highly reactive halenium (I$^+$) ion allowing iodine(I) complexes, such [bis(pyridine)iodine (I)]BF_4 (Barluenga's reagent) to be used as halogenating[32–34] and oxidising agents[35] in organic synthesis. Over the last decade, the $^+$I–N XBs in [N–I–N]$^+$ has received much attention[36] and they are now being utilized for constructing capsules,[37,38] helicates[39] and metal–organic frameworks (MOFs)[40] unrestrained homoleptic[41,42] and heteroleptic[43–45] and hierarchical,[46] and nucleophilic interactions of iodine(I) complexes,[47–49] as well as stable non-chiral[50–52] and chiral carbonyl hypoiodites.[53] Compared to the much more explored C–I···N XB systems,[44] oxygen atom as an XB acceptor has not attracted so much intention due to its lower nucleophilicity and inherent polydentate nature and electron "push-pull" property (Figure 2). However, the significance of X···O(carbonyl/ether) interactions has been demonstrated in protein-drug complexes[54,55] and crystal engineering.[56–64] These X···O interactions can be classified as weak and moderate XBs with interaction energies 0.5–20 kJ mol^{-1} and ~20–60 kJ mol^{-1}, respectively. Compared to XB research on X···N, X···O systems that utilize pyridine *N*-oxides (PyNOs), the oxidised products of the parent pyridines, as the XB acceptors in C–I···$^-$O–N$^+$ or N–I···$^-$O–N$^+$ systems is surprisingly scarce.[65–76]

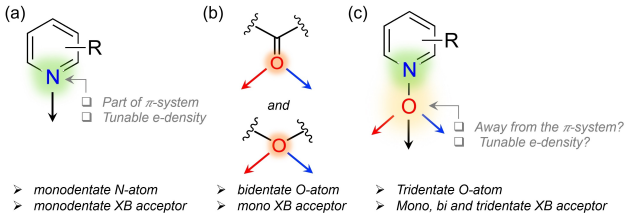

Figure 2. Depiction of electron-acceptor character of the (a) pyridinic N atom, (b) carbonyl and ether containing O systems, and (c) pyridine *N*-oxide O atom.

In our earlier contributions, we have investigated moderate strength C–I···$^-$O–N$^+$ XBs involving 1,*n*-perfluoroalkyliodoalkanes and PyNOs,[72] as well as strong N–I···$^-$O–N$^+$ XBs generated by *N*-halosaccharins and *N*-oxides (Figure 3).[76] The C–I···$^-$O–N$^+$ systems[52] have interaction energies ranging from 31.9 to 46.5 kJ mol^{-1},[69] while the N–I···$^-$O–N$^+$ have values ranging from 47.5 to 120.3 kJ mol^{-1}. The strongest N–I···$^-$O–N$^+$ XBs (120.3 kJ mol^{-1})[76] approach in strength the extremely strong [N–X–N]$^+$ XBs, being nearly equal to the values observed (> 160 kJ mol^{-1})[36] for the 3-*center*-4-*electron* [N–X–N]$^+$ (X = Br,I) halogen bonds in Barluenga-type halogen(I) complexes. In related systems *N*-haloimide/halosulfonimide XB donors have been utilized by Fourmigué et al.[77,78] Cinčić et al.[79–81] and others[82] to make complexes with pyridines as XB acceptors.

Our attempts[74] to tune the N–I···$^-$O–N$^+$ XB strengths using a broad selection of aromatic *N*-oxides, showed that the influence of changing *N*-oxide to the XB strengths is limited compared to the choice of XB donors in C–I···$^-$O–N$^+$ or N–I···$^-$O–N$^+$ systems. For example, titration study of 2-methyl-, 4-phenyl-, 2-methyl-4-nitro-, and parent pyridine *N*-oxide with *N*-iodosuccinimide (NIS) gave association constants (K_{XB}) of 779, 325, 17, and 660 M^{-1}, respectively, while the same N-oxides with stronger XB-donor *N*-iodosaccharin (NISac) gave K_{XB} values of 16338, 14200, 543, and 3121 M^{-1}. These K_{XB} values accurately follow the value of the σ-hole of NIS and NISac, respectively. Due to this we became intrigued to investigate to which extent the N–I···$^-$O–N$^+$ XBs can be tuned by choice of XB donor, namely the *N*-haloimides. In this study, we prepared a large family of XBs complexes from six *N*-haloimides and 27 PyNOs (Figure 3) to examine the structures and strengths of N–I···$^-$O–N$^+$ XBs. We chose PyNOs with methyl-, methoxy- and phenyl-substituents in *ortho*-, *meta*- and *para*-positions at the pyridine-*N*-oxide. The present work is an expansion of our earlier work[76] on similar system and employs *N*-haloimides because, the

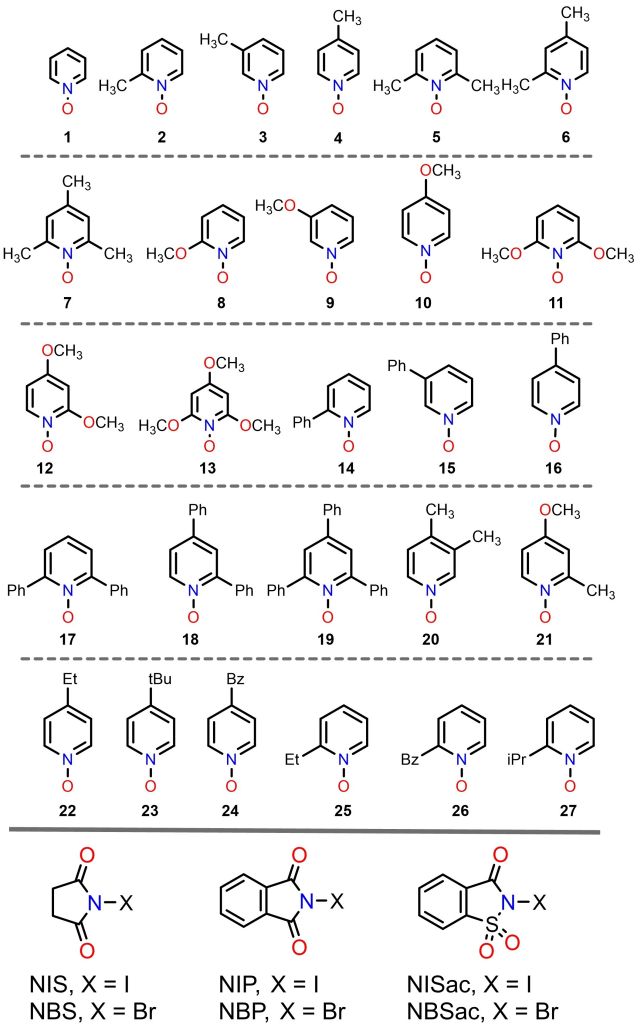

Figure 3. The chemical structures of the used components. The aromatic *N*-oxides (**1**–**27**) as XB acceptors and *N*-haloimides as XB donors: *N*-iodosuccinimide (NIS), *N*-bromosuccinimide (NBS), *N*-iodophthalimide (NIP), *N*-bromophthalimide (NBP), *N*-iodosaccharin (NISac), and *N*-bromosaccharin (NBSac).

$^{\delta-}$N–X$^{\delta+}$ bonds, though being strongly polarized, can tolerate the high nucleophilicity of *N*-oxides, and this enables us to measure the binding affinities of N–X···$^{-}$O–N^{+} motifs also in solution.

Results and Discussion

Computational Studies

In our earlier study on 54 *N*-halosaccharin-PyNO XB complexes,[76] we found that combining the local positive maxima of the electrostatic potential ($V_{S,max}$) of the XB donor halogen, the atomic charge (Q) and inverse of the average local ionization energies ($1/I_{S,min}$) of the XB acceptor oxygen of PyNOs allows a simple method of prediction of XB interaction energies (ΔE). This simple electrostatic model (named here as SiElMo) estimates the ΔE as:

$$\Delta E_{\mathrm{SiElMo}} = 0.95(V_{S,max} \times Q) - 1760 \times 1/I_{S,min} + 220$$

The above study also revealed that 22 of the DFT optimized XB structures manifest, in addition to the principal halogen bonding, secondary intramolecular interactions such as C–H···O=C and C–H···π that further stabilize the complexes and cause biased XB interaction energies calculated using DFT methods ΔE_{DFT}, leading to their exclusion from the SiElMo model. The strong correlation between the $V_{s,max}$ value describing the extent of halogen σ-hole and the strength of the XB, namely the donor halogen with larger $V_{s,max}$ value forming stronger XBs has been observed in halo-perfluoroalkanes/aromatics and N/O/S-heterocycles. For the *N*-haloimide XB donors of the current study, the calculated $V_{s,max}$ values (Figure 4a) unambiguously confirm the expected XB donor strength order of: NISac > NIS > NIP and NBSac > NBS > NBP. The $V_{s,max}$ for NISac (+186 kJ mol^{-1}) and NBSac (+142 kJ mol^{-1}) are higher than those of commonly used perfluorohalobenzene donors, e.g.,

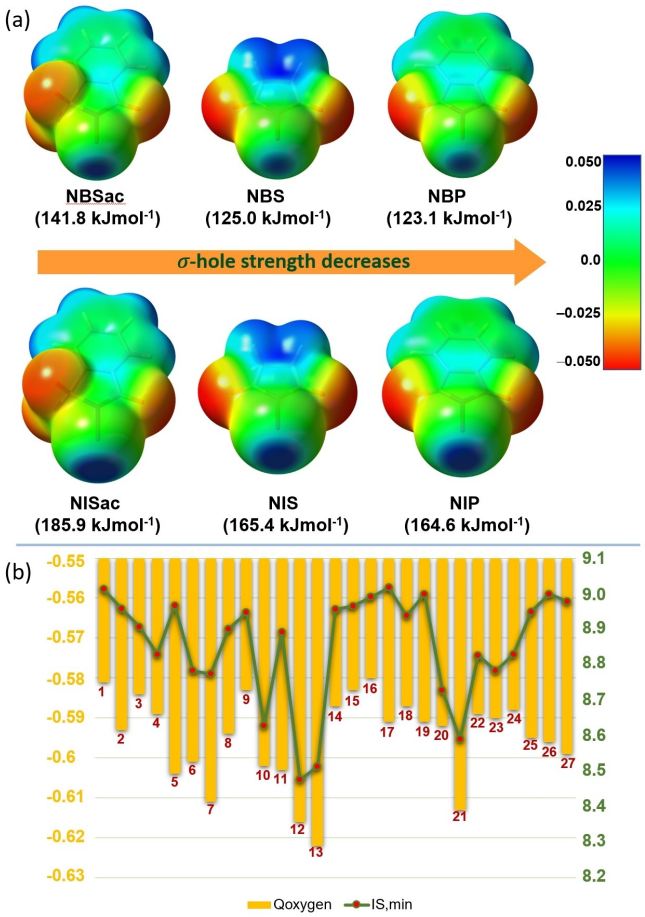

Figure 4. (a) Computed electrostatic potential surface (ESP) at the PBE0-D3/def2-TZVP level projected on the 0.001 au electron density surfaces of *N*-haloimides with $V_{S,max}$ values, NBSac, NBS, NBP (top: left-to-right), and NISac, NIS, and NIP (below: left-to-right). (b) Chart showing atomic charge (Q) and local ionisation energy ($I_{S,min}$) of the pyridine *N*-oxides' oxygen atom. Color code: Q (orange bars), $I_{S,min}$ (eV) (green line + red dots), and pyridine *N*-oxides (maroon numbers).

C_6F_5I (+134 kJ mol^{-1}) and C_6F_5Br (+100 kJ mol^{-1}).[83] The NIS and NBS have slightly higher $V_{s,max}$ values than their corresponding NIP and NBP counterparts with differences of 0.8 and 1.9 kJ mol^{-1}, respectively.

In the literature, some success has been achieved in describing the influence of the XB acceptor to the XB strength using minimum value of the surface electrostatic potential, $V_{s,min}$.[84–86] However, on the NISac and NBSac complexes our observation[76] was that the $V_{s,min}$ values do not lead to best possible correlation with the XB ΔE_{DFT} values. Instead, the Q value of the *N*-oxide oxygen (Figure 4b) appeared to be a better description of the acceptor's role in the formation of halogen bonds. The poor performance of $V_{s,min}$ alone can be attributed to the position of the $V_{s,min}$ of the oxygen atom, which is not coinciding with the direction of the halogen bond.[76] A smaller but significant contribution to the XB strengths comes from the reciprocal value of the minima of the average local ionization energies, $I_{S,min}$ (Figure 4b), of the XB acceptor oxygen, that describes how easily the XB acceptor molecules are polarized during the XB formation. Interaction energies for 90 XB complexes were predicted using SiElMo equation[76] (see above) together with $V_{S,max}$, Q, and $I_{S,min}$ values obtained from PBE0-D3/def2-TZVP calculations and correlated with the XB interaction energies calculated at PBE0-D3/def2-TZVP level of theory for optimized complex structures as shown in Figure 5 (See Supporting Information S2.1 for details). Applying such a simple electrostatic model (SiElMo) a surprisingly good linear correlation between SiElMo estimated and PBE0 calculated energies is observed (R^2= 0.963). Refitting of the SiElMo equation to the full dataset of all 90 XB complexes calculated with PBE0-D3/def2-TZVP method does not significantly change the correlation between the ΔE_{SiElMo} and ΔE_{DFT} [Figure S12 (SI Page 14), R^2 = 0.964], demonstrating the robustness of the SiElMo model.

Furthermore, similar observations of a strong linear link between SiElMo energies and ΔE_{DFT} are obtained when comparing ΔE_{DFT} calculated with the more demanding ωB97X-D/aug-cc-pVTZ(PP) DFT method and SiElMo using the original equation R^2 = 0.983 [Figure S13 (SI page 14)] or an equation refitted to the full dataset R^2 = 0.984 [Figure S14 (SI Page 15)]. Both ΔE_{SiElMo} and ΔE_{DFT} rank the interaction strengths of *N*-haloimide complexes as expected: NISac > NIS ≧ NIP > NBSac > NBS ≧ NBP. The simple SiElMo model from the small data set (32 complexes[76]) is able to predict XB interaction energies of all 90 XB complexes remarkably well.

The SiElMo model's success in estimating XB interaction energies indicates that ΔE′s are largely influenced by the $V_{s,max}$ of the halogen atom, while being affected to lesser extent by the Q-value of the *N*-oxide oxygen. The apparent strong influence of $V_{s,max}$ to XB interaction energies stems from the difference changing the identity of XB donor atom from iodine to bromine causes. If the changes to XB interaction energies caused by replacing the *N*-iodoimide by a different *N*-iodoimide are compared to the changes caused by varying the substituents in PyNOs the maximum changes that can be affected are very similar. As an example, interaction energies ΔE_{DFT} of NISac-**1** and NISac-**21**[76] are −65 and −85 kJ mol^{-1}, while for NIS-**1** and NIS-**21** they are −52 and −67 kJ mol^{-1}, respectively. Thus, changing the XB donor in complexes of **1** and **21** changes ΔE_{DFT} by 13 and 18 kJ mol^{-1}, respectively. By contrast, with the same com-

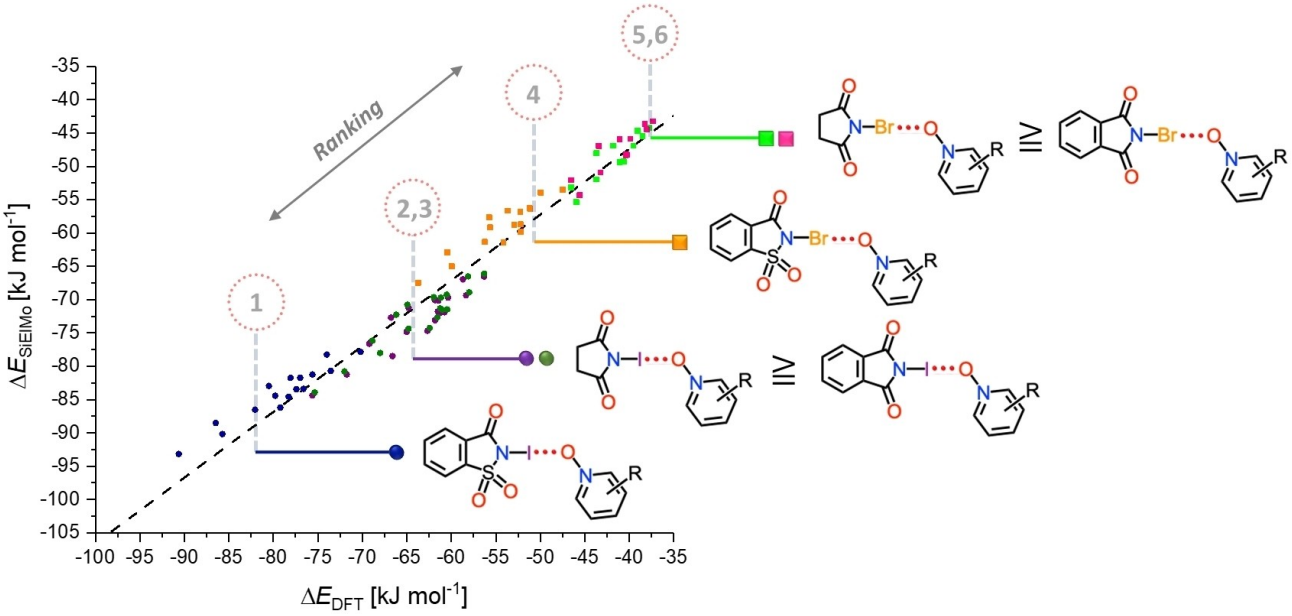

Figure 5. Linear correlation between XB interaction energies of 90 XB complexes calculated with the simple electrostatic model ΔE_{SiElMo} [=0.95 ($Q_{oxygen} \times V_{S,max}$)−1760×1/$I_{S,min}$(oxygen) + 220] and those calculated at the PBE0-D3/def2-TZVP level of theory for optimized structures (R^2 = 0.963). Color code: NIS (purple dots), NIP (olive dots), NISac (blue dots), NBS (bright green squares), NBP (pink squares), and NBSac (orange squares) complexes. The computed ΔE_{DFT} values for NISac/NBSac complexes are taken from our earlier work.[76]

plexes the change of XB acceptor in NIS and NISac complexes changes ΔE_{DFT} by 15 and 20 kJ mol^{-1}, respectively.

X-Ray Crystallography

Seventy-five crystal structures were assessed in order to understand the halogen bonding properties through the oxygen atom of the *N*-oxide, namely the elongation of N–X bond with simultaneous shortening of the N–X···$^{-}$O–N^{+} halogen bond. Close inspection of the X-ray structures reveals that the asymmetric units' of 61/75 structures contain one 1:1 XB complex, whereas the others feature deviations from the 1:1 stoichiometry. In these 14 other structures the N–X···$^{-}$O–N^{+} distances are nearly the same as in the 1:1 structures, differing only, at maximum, by 0.06 Å, For example, the asymmetric unit of NIS-**3** contains four crystallographically independent 1:1 complexes, whose N–I···$^{-}$O–N^{+} distances are 2.407(3), 2.434(3), 2.443(3), and 2.453(3) Å. As common feature to all the complexes N–X···$^{-}$O–N^{+} contact distance is markedly shorter than the sum of the van der Waals radii of X- and O-atoms and the contact is associated with elongated imide N–X bond, and N–X···$^{-}$O–N^{+} angle that is close to 180 degrees [See Tables S16–S21]. For the studied iodoimide-PyNO complexes the N–I···$^{-}$O–N^{+} halogen bond lengths range from 2.276(2) to 2.584(5) Å and for bromoimide-PyNO complexes the corresponding N–Br···$^{-}$O–N^{+} distances are from 2.217(2) to 2.509(3) Å. The NIS-**20** [2.354(3) Å, $R_{XB}=0.67$] of the NIS series, NIP-**2** [2.392(2) Å, $R_{XB}=0.68$] for the NIP and NISac-**5** [2.276(2) Å, $R_{XB}=0.65$][76] for the NISac manifest the shortest N–I···$^{-}$O–N^{+} XB distances. The NBS-**8** [2.34 Å, $R_{XB}=0.69$] for NBS, NBP-**20** [2.323(4) Å, $R_{XB}=0.69$] for NBP and NBSac-**20** (2.217(2) Å, $R_{XB}=0.66$][76] for NBSac exhibit the shortest Br···O distances. The R_{XB} values of the *N*-halosuccinimide and *N*-halosaccharin complexes are only slightly larger than the R_{HB} values of the corresponding *N*-imide-PyNO hydrogen-bonded complexes [Figure S15 (SI Page 31)].

In N–H···N$_{Py}$ and N–X···N$_{Py}$ complexes the pyridine nitrogen interacts with one donor through only one hydrogen or halogen bond. In contrast, the oxygen in the *N*-oxide has a multidentate acceptor capability and can interact to either one XB or HB donor (monodentate), one XB and HB donor or two XB donors (bidentate) or one XB and two HB donors (tridentate) simultaneously as depicted in Figures 6a–d. The crystal packing analysis of the 75 single crystal X-ray structures reveal that the *N*-oxide oxygen manifests the monodentate interaction (one N–X···$^{-}$O–N^{+} XB) in only one of the 75 structures. The others exhibit multidentate interaction patterns with μ_2-*O*,*O* in 6/75 (two N–X··· $^{-}$O–N^{+} XBs), μ_2-*O*,*O* in 48/75 (one N–X···$^{-}$O–N^{+} XB, one C–H···$^{-}$O–N^{+} HB), and μ_3-*O*,*O*,*O* in 22/75 (one N–X···$^{-}$O–N^{+} XB and two C–H···$^{-}$O–N^{+} HBs). Packing forces are responsible for the multidentate C–H···$^{-}$O–N^{+} interactions and, they play a critical role in the stabilization of XB complexes in the solid-state. The significance of C–H···$^{-}$O–N^{+} interactions involving PyNOs has previously been emphasized in crystal engineering studies.[87–91] The asymmetric units in two of the 75 structures, NIS-**20** and NBSac-**23**, have a second imide that is not involved in N–X···$^{-}$O–N^{+} halogen bonding. The second imide N–X forms N–X···O=C type XBs to the C=O of the NIS-**20** and NBSac-**23** complexes [Figure S16 (SI Page 31)].

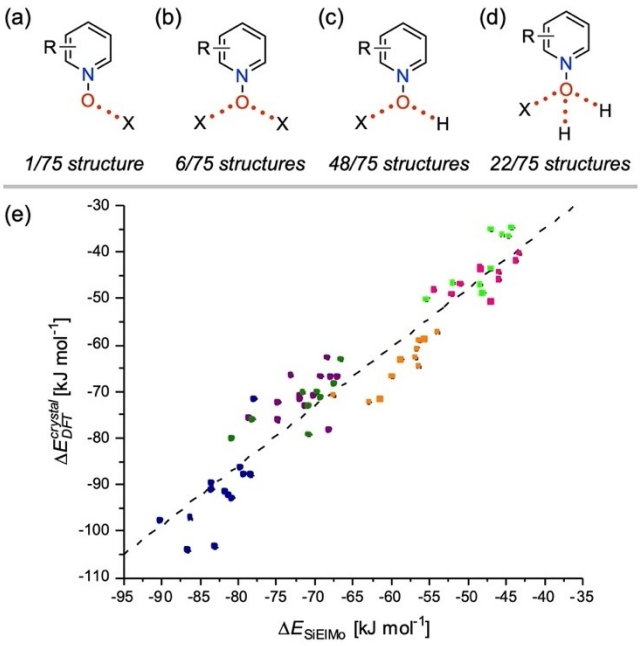

Figure 6. (a-d) Halogen and hydrogen monodentate and multifurcated modes of PyNOs (X = Br/I of imide, H = hydrogen of H–C). (e) Correlation plot of the XB interaction energies calculated at the PBE0-D3/def2-TZVP level of theory in the crystal-structure geometry $\Delta E_{DFT}^{crystal}$ and predicted with the simple model ΔE_{SiElMo} ($R^2=0.906$) for 66 monodentate *N*-haloimide PyNO XB complexes. Color legend: NBS (green squares), NBP (pink squares), NBSac (orange squares), NIS (purple dots), NIP (olive dots), and NISac (blue dots).

Given the good performance of the SiElMo model in reproducing the ΔE_{DFT} of the optimized structures we chose to test the energies predicted by the SiElMo against interaction energies calculated for crystal structure geometries $\Delta E_{DFT}^{crystal}$ with PBE0-D3/def2-TZVP method. The linear correlation between ΔE_{SiElMo} and $\Delta E_{DFT}^{crystal}$ ($R^2=0.906$) demonstrates that the model can be reliably used to predict general energy trends in the solid-state structures of *N*-haloimide PyNO XB complexes (Figure 6e). The same level of linear correlation is observed for the ΔE_{DFT}^{opt} of optimized structures and $\Delta E_{DFT}^{crystal}$ [Figure S9 (SI Page 10)] inferring that the XB are likely to retain their dominant structure directing role in also the solid-state structures.

The lengthening of the N–X bond occurs upon XB formation [Tables S16–S21 (SI Pages 28–30) and Figure S17 (SI Page 32)]. The imide N–X bond elongation defined as, $\Delta(N–X)=(N–X)_{complex}–(N–X)_{ligand}$, is in the range of 0.016–0.05 Å for NBS, 0.018–0.058 Å for NBP, 0.048–0.12 Å for NBSac, 0.005–0.056 Å for NIS, 0.05–0.07 Å for NIP and 0.069–0.114 Å for NISac complexes. The Δ(N–X) values are clearly larger for donors with larger $V_{S,max}$ (bigger σ-hole). It is generally accepted that in D–X···A halogen-bonded

complexes, the $(D–X)_{complex}$ bond lengths are longer than the $(D–X)_{ligand}$, and the $(D–X)_{complex}$ lengthening increases with decreasing X···A halogen bond lengths. The complexes with additional XB and/or HB contacts shown in Figure 6a–d suggest that the additional N–X···$^{-}$O–N^{+} and C–H···$^{-}$O–N^{+} interactions could have a major role in stabilizing the crystal lattice of the 1:1 donor:acceptor XB complexes. If this is the case, there should not be a direct relationship between N–X and X···O distances. To investigate this, we compiled and plotted the N–X distances as a function of X···O values observed in crystal structures of the XB complexes (Figure 7).

Overall, the N–X elongations and X···O distances with a slope of −3.49 for Br···O and −2.36 for I···O halogen bonds manifest a moderate correlation $R^2=0.866$ for the Br and $R^2=0.842$ for the I complexes. The negative slope indicates an inverse relationship, namely the N–X bond length increases while the X···O distance decreases. The Br···O and I···O distances group based on the $V_{s,max}$ values. Stronger XBs observed for the NBSac and NISac complexes, show a distance variation from 2.22 to 2.35 Å and 2.28 to 2.35 Å, respectively, forming well separated sets. The $V_{s,max}$ values of bromine in NBS and NBP and of iodine in NIS and NIP complexes differ only by ~2 kJ mol^{-1}. As a result, the X···O distances of the NBS and NBP, and NIS and NIP complexes are populated in narrow range of 2.37–2.51 Å and 2.38–2.46 Å, respectively, and do not form clearly distinguishable sets as the NBSac and NISac complexes do. Further, the weak and bifurcated I···O contacts manifest themselves as a separate set for the NISac complexes. The monodentate and bifurcated Br···O distances are comparable, and their groups diffuse into one another. The X···O distances seem unaffected by the non-XB interactions such as C–H···$^{-}$O–N^{+} HBs and depend more on the $V_{s,max}$ values indicating that the N–X···$^{-}$O–N^{+} motifs involving *N*-haloimides and PyNOs are robust in the solid-state.

Unlike in hypoiodite complexes[50] and Barluenga-type iodine(I) complexes[41,92] it is not possible to achieve a symmetric N–X–O halogen-bonded system using *N*-haloimides and PyNOs, as the iodine(I) cannot "jump" to the oxygen atom of the *N*-oxide. In their HB study Steiner et al. plotted O–H···N and O–H···O distances against O···N and O···O distances in O–H···N and O–H···O hydrogen-bonded systems. Plotting O···N and O···O distances as a function of O–H···N and O–H···O distances results in a curved path, where the midpoint of the curve corresponds to symmetric O···H···N and O···H···O bonding.[8] For instance, in the correlation of O–H and H···O distances against O···N separations, the O–H bond continuously elongates with decreasing H···O distance until a symmetric geometry for O–H–N is reached at O···N separation of about ~2.50 Å. In this situation, the distance of the H-atom from the N and O-atoms is 1.25 Å. Analogous methodology can be used to evaluate the symmetry of a N–X–O halogen-bonded system. Plots of N–X and X···O versus (imide)N···O(PyNO) distances for *N*-iodoimide and *N*-bromoimide complexes, respectively, are shown in Figure 8a and 8b. The plots of N···O distances as the function of N–X and X···O distances forms a parabolic curve where the two values approach a common minimum with N–X=O–N. The parabolic curve reaches minimum at a N···O distance of ~4.1 Å for bromoimide-PyNO complexes and ~4.4 Å for iodoimide-PyNO complexes. Although haloimide-*N*-oxide systems cannot reach this symmetric N–X–O bonding situation the distances for hypothetical symmetrical system are comparable to the distances found in carbonyl hypoiodite [4-bromobenzoate-DMAP-iodine(I)] complex where both N–X and X–O bond lengths are 2.22 Å with an N···O separation of 4.43 Å (Figure 8c).[50] This is possible as the pyridinic nitrogen atom can accept the iodine cation, resulting in the unstable iodopyridinium cation (which is then stabilized by the 4-bromobenzoate anion). The iodine cation can even jump to the pyridinic N atom, as happens in trifluoroacetate-DMAP-iodine(I) hypoiodite complex with I–N 2.173(4) and O···I 2.312 Å and O···N of 4.49 Å (Figure 8e).

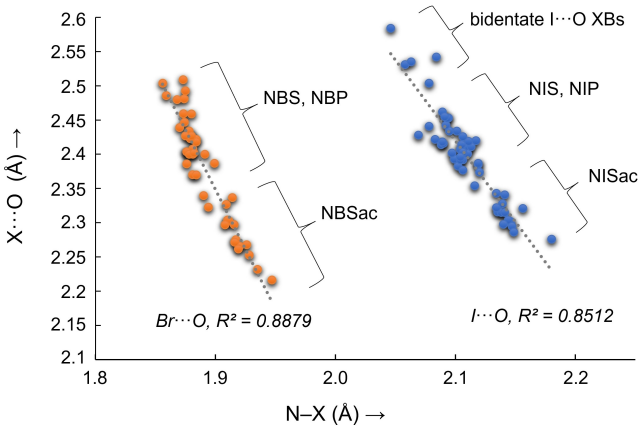

Figure 7. Correlation of X···O versus N–X distances in the single-crystalline XB complexes.

Solution Studies

Solution ^{15}N NMR Studies

The computational study of NIS-**1**, for example, indicates that the atomic charges on nitrogen of NIS, and nitrogen and oxygen atoms of **1**, become more negative upon XB complexation (Figure 9), suggesting that monitoring the NMR changes of oxygen and nitrogen atoms in solution could be used to evaluate complexation strength. However, the NMR active oxygen isotope ^{17}O has a natural abundance of only 0.035 %, which makes the ^{17}O NMR analysis challenging. On the other hand, the active isotope of nitrogen, ^{15}N, has a natural abundance of 0.37 %, making it suitable for ^{15}N NMR study.

The ^{15}N NMR coordination shift, $\delta^{15}N_{coord}$, defined as the difference between the chemical shift of a complexed ligand ($\delta^{15}N_{compl}$) and its uncomplexed form ($\delta^{15}N_{ligand}$), is a useful method for estimating the strength of coordination bonds. A larger absolute coordination shift, $|\Delta\delta^{15}N_{coord}|=\delta^{15}N_{compl}-\delta^{15}N_{ligand}$ indicates a stronger bond. It has previously been

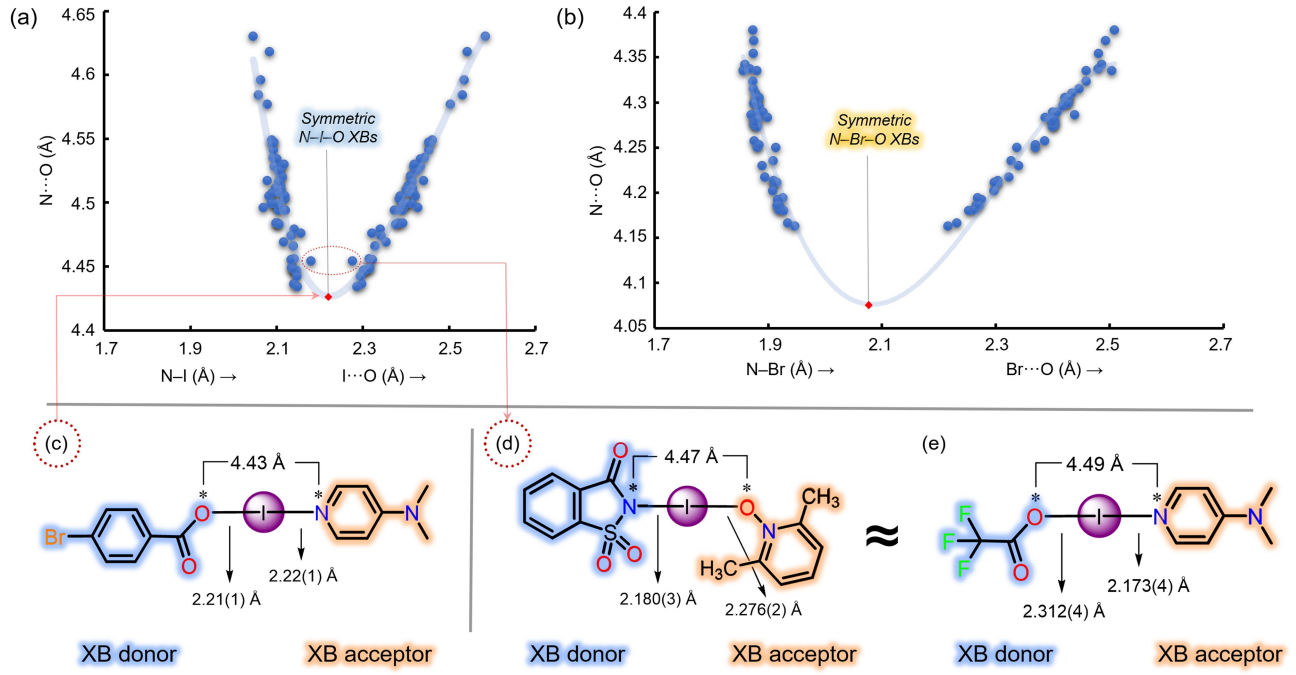

Figure 8. Solid-state X-ray crystal structures data. Correlation of (a) N–I and I···O versus (imide)N···O(PyNO), and (b) N–Br and Br···O versus (imide)N···O(PyNO). (c) Halogen-bonded symmetric situation of COO^- ···I–N^+ ion-pair (salt) in an asymmetric (DMAP)N–I–O(4-bromobenzoate) moiety, and (d and e) a comparable asymmetric situation of NISac-**5** (the strongest XB complex) and COO^- ···I–N^+ ion-pair (salt) in (DMAP)N–I–O (trifluoroacetate) moiety.

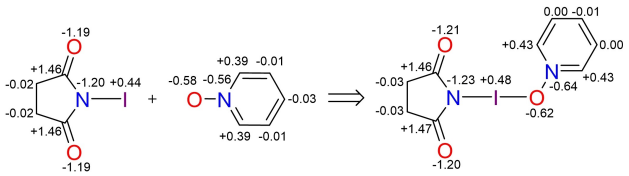

Figure 9. Chemdraw representation showing changes in the QTAIM atomic charges on formation of 1 : 1 XB adduct NIS-**1**.

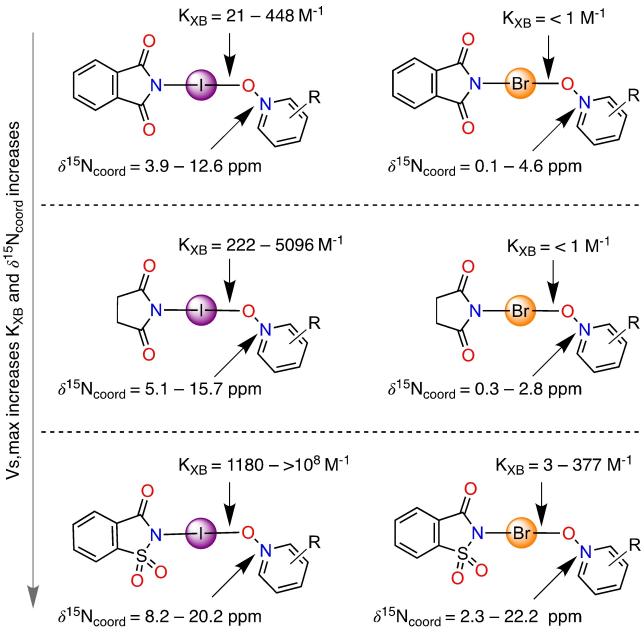

Figure 10. Summary of solution NMR K_{XB} and $\Delta\delta^{15}N_{coord}$ values.

used to describe the halogen bonding strengths and confirm complexations of Barluenga-type $[N–X–N]^+$[36] and carbonyl hypoiodite complexes C(O)–O–I–N_{Py}.[50–52] The ^{15}N NMR data was acquired to determine whether the $\Delta\delta^{15}N_{coord}$ of the nitrogen of PyNO and XB donor would follow the $V_{s,max}$ values of the halogens. For NIS and NBS complexes, determining $\Delta\delta^{15}N_{coord}$ was successful, but lack of protons at the 3-position in other XB donors prevented the determination in others. The successful estimation of $\Delta\delta^{15}N_{coord}$ of *N*-oxide nitrogen atom for all PyNOs was achieved and their $\Delta\delta^{15}N_{coord}$ values were used to compare the relative strengths of X···O halogen bonds. The stronger the X···O interaction, the larger the $\Delta\delta^{15}N_{coord}$ of the PyNO nitrogen atom. The $\Delta\delta^{15}N_{coord}$ values of NIS, NIP, NISac, NBS, NBP, and NBSac complexes are in the ranges of 5.1–15.7 ppm, 3.9–12.6 ppm, 8.2–20.2 ppm, 0.3–2.8 ppm, 0.1–4.6 ppm and 2.3–22.2 ppm, respectively (Figure 10). The magnitude of PyNOs' nitrogen $\Delta\delta^{15}N_{coord}$ values of the *N*-haloimide-PyNO complexes follow the sequence of haloimide halogen $V_{s,max}$ values, NISac > NIS > NIP for the I···O XBs. However, there are significant uncertainties in ranking the Br···O XBs using the $\Delta\delta^{15}N_{coord}$ values of PyNO nitrogen due to weak binding observed for the NBS and NBP complexes (Tables S51–53, Supporting Information pages 207–209).The above findings are also consistent with the observation that as the halogen size

decreases, it's XB donor properties (diminishing $V_{s,max}$ values) also decrease i.e., I > Br > Cl > F.[93]

Solution ^{1}H NMR Association Constants

The scope of our preliminary work[76] was further extended to include the solution NMR association constants (K_{XB}) of NIS and NIP complexes. By combining the previous[76] and the current results, plotting the binding constants between different *N*-haloimides with the 27 *N*-oxides allows evaluation of the solution behaviour in the *N*-haloimide-PyNO complexes (Figure 11). The K_{XB}'s were determined from changes in NISac and NBSac proton resonances caused by the XB complexation. With the use of HypNMR2006[94,95] and the online Bindfit[96] programs, the K_{XB} values were determined for a 1:1 donor-acceptor model (Table S54, Supporting Information page 210).

At 298 K the K_{XB} values of NIS complexes in $CDCl_3$ range from 222 to 6434 M^{-1}, and of NIP complexes from 20 to 448 M^{-1}. Titrations of NIS complexes were also carried out in XB competing solvent, [D_6]acetone, since some of the K_{XB} values of NIS complexes in $CDCl_3$ manifest high fitting errors. When compared to $CDCl_3$, the K_{XB} values of NIS complexes in [D_6]acetone are smaller and range from 2 to 945 M^{-1}, with small fitting errors. The K_{XB} values of the NIS and NIP complexes were smaller than those for NISac complexes, which varied between 1180 and $>10^8$ M^{-1}. Only the K_{XB} values of NBSac complexes were measurable at 298 K, whereas NBP and NBS complexes could not be measured due to weak binding. The K_{XB} values of NBS-**7** and NBP-**7** were measured at 273 K and 253 K to check if they follow the computed bromine $V_{s,max}$ values. The NBS-**7** has a K_{XB} value of 5 and 7 M^{-1} at 273 K and 253 K, respectively. Estimation of the K_{XB} for NBP-**7** at 273 K was unsuccessful as no chemical shift changes to the donor protons were observed, however binding was observed at 253 K, being 3 M^{-1}. The slightly larger K_{XB} of NBS-**7** than NBP-**7** clearly suggest that NBS is a stronger donor and NBP is a weaker XB donor, as determined by the computed bromine $V_{s,max}$ values (Figure 4a).

The logarithmic K_{XB} values of NISac, NIS, NIP and NBSac complexes, obtained in $CDCl_3$, were plotted for each XB acceptor separately (Figure 11), revealing interesting trends. Figure 11 provides some useful insights: (i) The average K_{XB} values of all complexes follow the $V_{s,max}$ of the XB donor. It should be noted that the very high $K_{XB,}$ and very likely erroneous, value for NISac-**7** ($>10^8$) has been excluded from the average. The bromine-atom donor series of NBSac complexes with Br···O XBs shows weak, but consistent, binding. (ii) The strongest I···O XBs occurring for NISac complexes have a conspicuously random distribution of the K_{XB} values, whereas weaker I···O XBs for NIS and NIP complexes have a more ''steady'' distribution. This observation suggests that the simple interpretation of relating the chemical shift changes directly to K_{XB} association constants might break for the complexes of XB donors with the largest $V_{s,max}$ values and the observed changes are

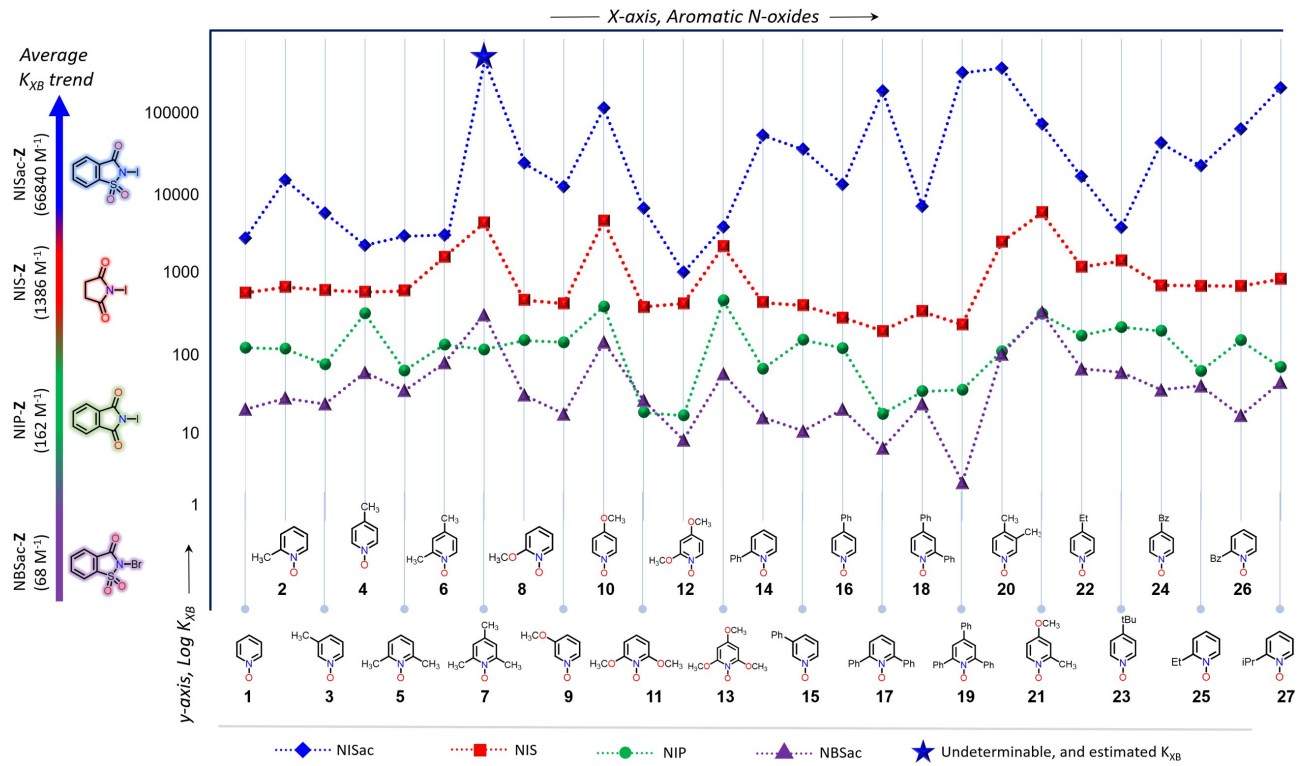

Figure 11. Chart displaying K_{XB} values trend of NISac-**Z** (blue diamonds), NIS-**Z** (red squares), NIP-**Z** (green dots), and NBSac-**Z** (olive triangles). The K_{XB} value of the NISac-**7** is unknown; the blue star indicates the estimated value but is excluded from the average.

likely to reflect decomposition and/or influence of secondary interactions as well. These factors could explain the erratic pattern as well as large fitting errors to K_{XB} values of NISac complexes (Table S54, Supporting Information page 210).

Categories of Weak, Moderate, Strong N–X···$^{-}$O–N^{+} Halogen Bonds

We combine our data for helpful practical purposes to introduce indicators for the categories of weak, moderate, and strong XBs, as shown in Table 1. Interaction energies and X···O distances have no clear boundaries and numerical data should only be used as a general guide. Additionally, different donor-acceptor partners generate specific non-covalent bonds in solutions and crystals, and they rely on the functional groups in the donors and acceptors. A notable difference between categorization of HBs and XBs is that ∠N–X···O angles cannot be related to X···O distances in the same way as weak (>90°), moderate (>130°), and strong (170–180°) HBs separated into classes based on the angles.[97] For example, the strongest I···O of NISac-**5** [2.276 (2) Å, ∠N–I···O = 176.14(10)°] shows larger deviation from the linearity than the weakest I···O XB of NIS-**8** [2.584(5) Å, ∠N–I···O = 178.6(3)°], even though linearity is what is expected of strong XBs. The X-atom preference for high directionality can be attributed for the near linearity in all complexes [167.72(15)°–179.38(14)°, Tables S16–S21, Supporting Information pages 28–30], while packing forces are expected to account for the small variations in the bond angles.

Conclusion

Six *N*-haloimide XB donors and 27 pyridine *N*-oxide (PyNO) XB acceptors are studied for N–X···$^{-}$O–N^{+} (X = I, Br) halogen bonding interactions In silico, crystals, and solution with the aim of understanding their bonding nature. DFT XB interaction energies for *N*-iodoimide-PyNO complexes range from −56 to −120 kJ mol^{-1}, while for *N*-bromoimide-PyNO complexes, they are between −38 and −82 kJ mol^{-1}. These bond energies are the strongest of their kind but ≧40 kJmol^{-1} weaker than the well-known $^{+}$X···N XBs in [N–X–N]$^{+}$ halogen-bonded systems. A simple electrostatic model (SiElMo) is presented to predict the X···O XB bond energies from the properties of XB donor halogen and acceptor oxygen atoms. SiElMo uses the positive electrostatic surface potential of the donor halogen and the atomic charge and average local ionization energies of the PyNOs' oxygen. There is a strong correlation (R^2 = 0.963) between ΔE_{SiElMo} model energies and the halogen bond interaction energies ΔE_{DFT} determined from the DFT optimized structures of the complexes. Both the ΔE_{SiElMo} and ΔE_{DFT} rank the XB interaction strengths in the order: *N*-iodosaccharin > *N*-iodosuccinimide ≧ *N*-iodophthalimide > *N*-bromosaccharin > *N*-bromosuccinimide ≧ *N*-bromophthalimide. The X···O interaction energies calculated using crystal structure coordinates (ΔE_{DFT}^{cryst}) and ΔE_{SiElMo} show a strong linear correlation (R^2 = 0.902), demonstrating the robustness of the SiElMo model and proving that the XB interaction is the dominant non-covalent interaction motif that determines the *N*-haloimide-PyNO complexes. The success of using the SiElMo model, that was developed on a small training set, to predict the XB energies of a much larger set of complexes paves the way for using the model as an expedient way of characterizing X···O halogen bonds in larger systems such as biomolecules. The finding also raises the question if the model or similar model could be extended for other types of XBs as well.

In the solid-state, the X···O distances of *N*-iodoimide-PyNO complexes vary from 2.276(2) to 2.584(5) Å, whereas for *N*-bromoimide-PyNO complexes they range from 2.217(2) to 2.509(3) Å. The correlation between (imide)N–X *vs* X···O distances establishes a common link, that is, as the N–X bond lengthens, the X···O distance shortens. Within this correlation, the X···O halogen bonds form groups that can be ranked based on donor halogen sigma-hole strength, *N*-halosaccharin > *N*-halosuccinimide ≧ *N*-halophthalimide. *N*-iodosaccharin complexes have short X···O distances, with normalized interaction ratios (R_{XB}) ranging from 0.65 to 0.70, and hence are the shortest N–I···$^{-}$O–N^{+} halogen bonds of their class. These values are only minutely larger than the R_{XB} values of 0.64 observed for [bis(pyridine)iodine]$^{+}$ XB complexes. Out of 75 crystal structures, in only one structure, the *N*-oxide oxygen has a monodentate N–X···$^{-}$O–N^{+} XB bonding mode and the others exhibit multidentate interaction patterns with μ_2-*O*,*O* in 6/75 (two N–X···$^{-}$O–N^{+} XBs), μ_2-*O*,*O* in 48/75 (one N–X···$^{-}$O–N^{+} XB, one C–H···$^{-}$O–N^{+} HB), and μ_3-*O*,*O*,*O* in 22/75 (one N–X···$^{-}$O–N^{+} XB and two C–H···$^{-}$O–N^{+} HBs). This finding shows that the *N*-oxide oxygen's polydentate coordination nature plays a significant role in crystal packing processes and that in solution, the *N*-oxide oxygen may have a comparable or even higher tendency for polydenticity. In solution, the binding affinities can be significantly influenced by the solvation and entropy of the donor and acceptor molecules, which neither DFT nor crystal structures reflect. Although desirable, correlations between DFT/solid-state and solution are not seen. Solution NMR data are treated separately. Trends for NMR association constants have been calculated independently for each of the *N*-haloimide-PyNO families. *N*-iodosaccharin complexes with strong XB donor capacities exhibit erratic patterns of association constant distributions, whereas *N*-haloimide complexes with weak donor properties have more ''steady'' distributions. The association constants follow the sigma-hole strengths of XB

Table 1: Classification of strong, moderate, and weak N–X···$^{-}$O–N^{+} XBs.

	weak	moderate	Strong
X···O Bond length (Å)	>2.5	2.4–2.5	<2.3
N–X Lengthening	<0.05	0.05–0.09	>0.10
Bond energy (kJ mol^{-1})	<20	20–60	>60
Association constants (M^{-1})	1–99	100–1000	>1000

donors, which is in agreement with DFT and solid-state X-ray crystallography data.

Social media promotion

Halogen-bond energies were evaluated and classified using N-haloimides as halogen-bond donors and aromatic N-oxides as halogen-bond acceptors. The sigma-hole of the halogen in N-haloimides allows the quantification the bond strengths, and it is surprising how little oxygen impacts strengths.

Acknowledgements

The authors gratefully acknowledge financial support from the Academy of Finland (RP grant no. 298817, KR grant no. 351121), and provisions of computational resources by the Finnish Grid and Cloud Infrastructure (urn:nbn:fi:research-infras-2016072533) and Prof. Dr Heikki Tuononen (University of Jyväskylä).

Conflict of Interest

The authors declare no conflict of interest.

Data Availability Statement

The data that support the findings of this study are available from the corresponding author upon reasonable request.

Keywords: DFT · Halogen Bond · *N*-Haloimide · *N*-Oxide · X-Ray Structure

[1] M. Raynal, P. Ballester, A. Vidal-Ferran, P. W. N. M. Van Leeuwen, *Chem. Soc. Rev.* **2014**, *43*, 1660–1733.
[2] O. Yamauchi, *Phys. Sci. Rev.* **2019**, *1*, 20160001.
[3] S. Jena, J. Dutta, K. D. Tulsiyan, A. K. Sahu, S. S. Choudhury, H. S. Biswal, *Chem. Soc. Rev.* **2022**, *51*, 4261–4286.
[4] B. Alberts, *Molecular Biology of the Cell*, Garland Science, New York, **2002**.
[5] K. Müller-Dethlefs, P. Hobza, *Chem. Rev.* **2000**, *100*, 143–167.
[6] G. R. Desiraju, T. Steiner, *The Weak Hydrogen Bond: In Structural Chemistry and Biology*, Oxford University Press, **2001**.
[7] M. C. Etter, *Acc. Chem. Res.* **1990**, *23*, 120–126.
[8] T. Steiner, *Angew. Chem. Int. Ed.* **2002**, *41*, 48–76.
[9] S. J. Grabowski, *Chem. Rev.* **2011**, *111*, 2597–2625.
[10] *Hydrogen Bonding in Organic Synthesis* (Ed.: Petri M. Pihko), Wiley-VCH, Weinheim, **2009**.
[11] S.-W. Kuo, *Hydrogen Bonding in Polymeric Materials*, Wiley-VCH, Weinheim, **2018**.
[12] S. J. D. Lugger, S. J. A. Houben, Y. Foelen, M. G. Debije, A. P. H. J. Schenning, D. J. Mulder, *Chem. Rev.* **2022**, *122*, 4946–4975.
[13] G. R. Desiraju, P. Shing Ho, L. Kloo, A. C. Legon, R. Marquardt, P. Metrangolo, P. Politzer, G. Resnati, K. Rissanen, *Pure Appl. Chem.* **2013**, *85*, 1711–1713.
[14] E. Arunan, G. R. Desiraju, R. A. Klein, J. Sadlej, S. Scheiner, I. Alkorta, D. C. Clary, R. H. Crabtree, J. J. Dannenber, P. Hobza, H. G. Kjaergaard, A. C. Legon, B. Mennucci, D. J. Nesbitt, *Pure Appl. Chem.* **2011**, *83*, 1637–1641.
[15] K. Rissanen, *CrystEngComm* **2008**, *10*, 1107–1113.
[16] K. E. Riley, J. S. Murray, J. Fanfrlík, J. Řezáč, R. J. Solá, M. C. Concha, F. M. Ramos, P. Politzer, *J. Mol. Model.* **2011**, *17*, 3309–3318.
[17] T. Clark, M. Hennemann, J. S. Murray, P. Politzer, *J. Mol. Model.* **2007**, *13*, 291–296.
[18] P. Politzer, J. S. Murray, T. Clark, G. Resnati, *Phys. Chem. Chem. Phys.* **2017**, *19*, 32166–32178.
[19] Q. M. Dang, J. H. Simpson, C. A. Parish, M. C. Leopold, *J. Phys. Chem. A* **2021**, *125*, 9377–9393.
[20] P. Metrangolo, G. Resnati, *Halogen Bonding: Fundamentals and Applications*, Springer-Verlag, Berlin, **2008**.
[21] P. Metrangolo, G. Resnati, *Halogen Bonding: Impact on Material Chemistry and Life Sciences*, Springer International Publishing, Cham, **2015**.
[22] C. B. Aakeroy, D. L. Bryce, G. R. Desiraju, A. Frontera, A. C. Legon, F. Nicotra, K. Rissanen, S. Scheiner, G. Terraneo, P. Metrangolo, G. Resnati, *Pure Appl. Chem.* **2019**, *91*, 1889–1892.
[23] A. Bauzá, A. Frontera, *Angew. Chem. Int. Ed.* **2015**, *54*, 7340–7343.
[24] A. Bauzá, I. Alkorta, J. Elguero, T. J. Mooibroek, A. Frontera, *Angew. Chem. Int. Ed.* **2020**, *59*, 17482–17487.
[25] L. Brammer, *Faraday Discuss.* **2017**, *203*, 485–507.
[26] S. J. Grabowski, *Coord. Chem. Rev.* **2020**, *407*, 213171.
[27] L. Vogel, P. Wonner, S. M. Huber, *Angew. Chem. Int. Ed.* **2019**, *58*, 1880–1891.
[28] M. S. Taylor, *Coord. Chem. Rev.* **2020**, *413*, 213270.
[29] K. T. Mahmudov, A. V. Gurbanov, M. F. C. Guedes da Silva, A. J. L. Pombeiro, in *Noncovalent Interactions in Catalysis*, The Royal Society of Chemistry, Croydon, **2019**.
[30] *Noncovalent Forces* (Ed.: S. Scheiner), Springer International Publishing, Cham, **2015**.
[31] J. Zheng, A. Suwardi, C. J. E. Wong, X. J. Loh, Z. Li, *Nanoscale Adv.* **2021**, *3*, 6342–6357.
[32] G. Espuña, G. Arsequell, G. Valencia, J. Barluenga, J. M. Alvarez-Gutiérrez, A. Ballesteros, J. M. González, *Angew. Chem. Int. Ed.* **2004**, *43*, 325–329.
[33] J. Barluenga, H. Vázquez-Villa, A. Ballesteros, J. M. González, *J. Am. Chem. Soc.* **2003**, *125*, 9028–9029.
[34] J. Barluenga, M. Trincado, E. Rubio, J. M. González, *Angew. Chem. Int. Ed.* **2003**, *42*, 2406–2409.
[35] J. Barluenga, F. González-Bobes, M. C. Murguía, S. R. Ananthoju, J. M. González, *Chem. Eur. J.* **2004**, *10*, 4206–4213.
[36] L. Turunen, M. Erdélyi, *Chem. Soc. Rev.* **2020**, *49*, 2688–2700.
[37] L. Turunen, A. Peuronen, S. Forsblom, E. Kalenius, M. Lahtinen, K. Rissanen, *Chem. Eur. J.* **2017**, *23*, 11714–11718.
[38] L. Turunen, U. Warzok, C. A. Schalley, K. Rissanen, *Chem* **2017**, *3*, 861–869.
[39] A. Vanderkooy, A. K. Gupta, T. Földes, S. Lindblad, A. Orthaber, I. Pápai, M. Erdélyi, *Angew. Chem. Int. Ed.* **2019**, *58*, 9012–9016.
[40] G. Gong, S. Lv, J. Han, F. Xie, Q. Li, N. Xia, W. Zeng, Y. Chen, L. Wang, J. Wang, S. Chen, *Angew. Chem. Int. Ed.* **2021**, *60*, 14831–14835.
[41] A.-C. C. Carlsson, J. Gräfenstein, J. L. Laurila, J. Bergquist, M. Erdélyi, *Chem. Commun.* **2012**, *48*, 1458–1460.
[42] M. Bedin, A. Karim, M. Reitti, A.-C. C. Carlsson, F. Topić, M. Cetina, F. Pan, V. Havel, F. Al-Ameri, V. Sindelar, K.

Rissanen, J. Grafenstein, M. Erdelyi, *Chem. Sci.* **2015**, *6*, 3746–3756.
[43] J. S. Ward, G. Fiorini, A. Frontera, K. Rissanen, *Chem. Commun.* **2020**, *56*, 8428–8431.
[44] D. von der Heiden, K. Rissanen, M. Erdélyi, *Chem. Commun.* **2020**, *56*, 14431–14434.
[45] S. Yu, J. S. Ward, *Dalton Trans.* **2022**, *51*, 4668–4674.
[46] J. S. Ward, *CrystEngComm* **2022**, *24*, 7029–7033.
[47] S. Yu, P. Kumar, J. S. Ward, A. Frontera, K. Rissanen, *Chem* **2021**, *7*, 948–958.
[48] J. S. Ward, A. Frontera, K. Rissanen, *Inorg. Chem.* **2021**, *60*, 5383–5390.
[49] S. Wilcox, D. Sethio, J. S. Ward, A. Frontera, R. Lindh, K. Rissanen, M. Erdélyi, *Chem. Commun.* **2022**, *58*, 4977–4980.
[50] S. Yu, J. S. Ward, K. N. Truong, K. Rissanen, *Angew. Chem. Int. Ed.* **2021**, *60*, 20739–20743.
[51] E. Kramer, S. Yu, J. S. Ward, K. Rissanen, *Dalton Trans.* **2021**, *50*, 14990–14993.
[52] J. S. Ward, J. Martõnova, L. M. E. Wilson, E. Kramer, R. Aav, K. Rissanen, *Dalton Trans.* **2022**, *51*, 14646–14653.
[53] M. Mattila, K. Rissanen, J. S. Ward, *Chem. Commun.* **2023**, *59*, 4648–4651.
[54] R. Wilcken, M. O. Zimmermann, A. Lange, A. C. Joerger, F. M. Boeckler, *J. Med. Chem.* **2013**, *56*, 1363–1388.
[55] M. R. Scholfield, C. M. Vander Zanden, M. Carter, P. S. Ho, *Protein Sci.* **2013**, *22*, 139–152.
[56] M. T. Messina, P. Metrangolo, W. Panzeri, T. Pilati, G. Resnati, *Tetrahedron* **2001**, *57*, 8543–8550.
[57] C. B. Aakeröy, T. K. Wijethunga, J. Desper, *CrystEngComm* **2014**, *16*, 28–31.
[58] W. Borley, B. Watson, Y. P. Nizhnik, M. Zeller, S. V. Rosokha, *J. Phys. Chem. A* **2019**, *123*, 7113–7123.
[59] N. Bedeković, L. Fotović, V. Stilinović, D. Cinčić, *Cryst. Growth Des.* **2022**, *22*, 987–992.
[60] M. Benito, Y. Roselló, M. Barceló-Oliver, A. Frontera, E. Molins, *Int. J. Mol. Sci.* **2021**, *22*, 10663.
[61] V. Nemec, D. Cinčić, *Cryst. Growth Des.* **2022**, *22*, 5796–5801.
[62] K. M. Bairagi, K. S. Ingle, R. Bhowal, S. A. Mohurle, A. Hasija, O. I. Alwassil, K. N. Venugopala, D. Chopra, S. K. Nayak, *ChemPlusChem* **2021**, *86*, 1167–1176.
[63] V. V. Panikkattu, A. S. Huber, A. S. Sinha, B. B. Averkiev, C. B. Aakeröy, *Cryst. Growth Des.* **2022**, *22*, 1538–1542.
[64] V. Nemec, T. Piteša, T. Friščić, D. Cinčić, *Cryst. Growth Des.* **2020**, *20*, 3617–3624.
[65] W. X. Wu, H. Wang, W. J. Jin, *Cryst. Growth Des.* **2018**, *18*, 6742–6747.
[66] W. X. Wu, H. C. Liu, W. J. Jin, *Chem. Eur. J.* **2022**, *28*, e202103336.
[67] C. B. Aakeröy, T. K. Wijethunga, J. Desper, *CrystEngComm* **2014**, *16*, 28–31.
[68] W. X. Wu, H. Wang, W. J. Jin, *CrystEngComm* **2020**, *22*, 5649–5655.
[69] C. Cavallotti, P. Metrangolo, F. Meyer, F. Recupero, G. Resnati, *J. Phys. Chem. A* **2008**, *112*, 9911–9918.
[70] Y. P. Nizhnik, A. Sons, M. Zeller, S. V. Rosokha, *Cryst. Growth Des.* **2018**, *18*, 1198–1207.
[71] R. Liu, H. Wang, W. J. Jin, *Cryst Growth Des* **2017**, *17*, 3331–3337.
[72] R. Puttreddy, F. Topić, A. Valkonen, K. Rissanen, *Crystals (Basel)* **2017**, *7*, 214.
[73] G. R. Hanson, P. Jensen, J. McMurtrie, L. Rintoul, A. S. Micallef, *Chem. Eur. J.* **2009**, *15*, 4156–4164.
[74] R. Puttreddy, O. Jurcek, S. Bhowmik, T. Mäkelä, K. Rissanen, *Chem. Commun.* **2016**, *52*, 2338–2341.
[75] R. Puttreddy, N. K. Beyeh, K. Rissanen, *CrystEngComm* **2016**, *18*, 793–799.
[76] R. Puttreddy, J. M. Rautiainen, T. Mäkelä, K. Rissanen, *Angew. Chem. Int. Ed.* **2019**, *58*, 18610–18618.
[77] O. Makhotkina, J. Lieffrig, O. Jeannin, M. Fourmigué, E. Aubert, E. Espinosa, *Cryst. Growth Des.* **2015**, *15*, 3464–3473.
[78] E. Aubert, E. Espinosa, I. Nicolas, O. Jeannin, M. Fourmigué, *Faraday Discuss.* **2017**, *203*, 389–406.
[79] V. Stilinović, G. Horvat, T. Hrenar, V. Nemec, D. Cinčić, *Chem. Eur. J.* **2017**, *23*, 5244–5257.
[80] J. Mavračić, D. Cinčić, B. Kaitner, *CrystEngComm* **2016**, *18*, 3343–3346.
[81] M. Eraković, D. Cinčić, K. Molčanov, V. Stilinović, *Angew. Chem. Int. Ed.* **2019**, *131*, 15702–15706.
[82] I. Castellote, M. Morón, C. Burgos, J. Alvarez-Builla, A. Martin, P. Gómez-Sal, J. J. Vaquero, *Chem. Commun.* **2007**, 1281–1283.
[83] K. N. Truong, J. M. Rautiainen, K. Rissanen, R. Puttreddy, *Cryst. Growth Des.* **2020**, *20*, 5330–5337.
[84] I. Alkorta, G. Sánchez-Sanz, J. Elguero, *CrystEngComm* **2013**, *15*, 3178–3186.
[85] P. Politzer, J. S. Murray, T. Clark, *Phys. Chem. Chem. Phys.* **2013**, *15*, 11178–11189.
[86] J. S. Murray, P. Politzer, *Crystals* **2020**, *10*, 76.
[87] A. V. Shishkina, V. V. Zhurov, A. I. Stash, M. V. Vener, A. A. Pinkerton, V. G. Tsirelson, *Cryst. Growth Des.* **2013**, *13*, 816–828.
[88] A. J. Rybarczyk-Pirek, M. Łukomska-Rogala, K. Wzgarda-Raj, S. Wojtulewski, M. Palusiak, *Cryst. Growth Des.* **2018**, *18*, 7373–7382.
[89] L. M. Foroughi, A. J. Matzger, *Cryst. Growth Des.* **2021**, *21*, 5873–5879.
[90] N. J. Babu, L. S. Reddy, A. Nangia, *Mol. Pharm.* **2007**, *4*, 417–434.
[91] L. S. Reddy, N. J. Babu, A. Nangia, *Chem. Commun.* **2006**, 1369–1371.
[92] S. B. Hakkert, M. Erdélyi, *J. Phys. Org. Chem.* **2015**, *28*, 226–233.
[93] P. J. Costa, *Phys. Sci. Rev.* **2017**, *2*, 20170136.
[94] C. Frassineti, L. Alderighi, P. Gans, A. Sabatini, A. Vacca, S. Ghelli, *Anal. Bioanal. Chem.* **2003**, *376*, 1041–1052.
[95] C. Frassineti, S. Ghelli, P. Gans, A. Sabatini, M. S. Moruzzi, A. Vacca, *Anal. Bioanal. Chem.* **1995**, *231*, 374–382.
[96] P. Thordarson, *Chem. Soc. Rev.* **2011**, *40*, 1305–1323.
[97] G. Gilli, P. Gilli, *The Nature of the Hydrogen Bond: Outline of a Comprehensive Hydrogen Bond Theory*, Oxford University Press, Oxford, **2009**.

Manuscript received: May 25, 2023
Accepted manuscript online: June 14, 2023
Version of record online: June 14, 2023